Separation Of Long Polyelectrolytes In A Microfluidic Channel With Constrictions: A Monte Carlo Study

F. Tessier and G. W. Slater*

* Department of Physics, University of Ottawa, 150 Louis-Pasteur
Ottawa, Ontario, Canada, K1N 6N5
gslater@science.uottawa.ca

ABSTRACT

We present Monte Carlo simulation results for the motion of long linear polyelectrolytes inside a microchannel of molecular dimensions, structured as a periodic array of wells linked by narrow constrictions. Molecules are driven in the channel by a low-intensity electric field, which we model realistically by solving the Laplace equation numerically inside the channel. Our results agree with the counterintuitive experimental observation that longer molecules advance faster than shorter ones, and we show how this separation capability is related to the conformational changes of the molecule as it approaches a constriction. We further discuss possible improvements to the original channel design using pulsed fields, notably by exploiting ratchet operating modes and resonance effects. We support these new ideas with calculations in the zero-frequency limit and simulations in the finite frequency domain.

Keywords: microfluidics, electrophoresis, ratchet, DNA.

1 INTRODUCTION

The advent of microfluidics in the field of molecular biology offers exciting prospects. Current development focuses on DNA separation techniques (in an effort to optimize gene mapping and sequencing), but devices on which the preparation, sorting and detection of biomolecules is streamlined and integrated with analysis tools are already envisioned. Characterizing and understanding the behavior of biological molecules in small conduits is a necessary step towards this goal. The dynamics of these molecules — typically polymers — is quite different from that of simple fluids, as it is often dominated by their internal entropy. On the other hand, entropy represents a supplementary molecular variable one can exploit to achieve faster and better separations. This aspect has up to now been largely underestimated.

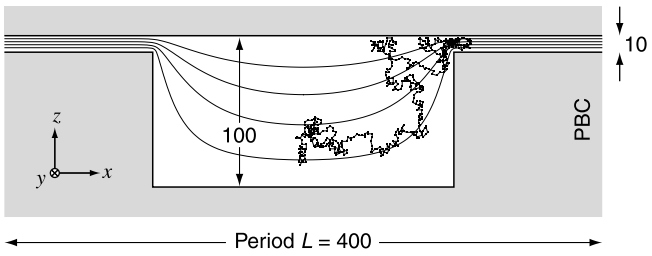

Figure 1: A two-dimensional side view of the channel structure used for the simulation. The field lines and a molecule of size $N = 600$ are shown.

In this paper we focus on a microchannel device fabricated by Han et al. (see figure 1) and recently used for the separation of double-stranded DNA (dsDNA) fragments by size, in the tens of kilobasepairs (kbp) range [1,2]. Molecules are electrophoresed through a series of traps by a constant (dc) electric field. We model this system with the bond-fluctuation algorithm in three dimensions [3,4]. We first investigate the behavior of the molecules in the dc regime, and then extend our work to the case of time-varying (ac) driving fields. In particular, we study whether strategies based on ratchet-like ideas [5,6] and resonance effects can lead to increased performance.

2 THEORY

Let us start by defining key quantities we will refer to throughout this note. Taking V as the global potential difference applied across the channel period of length L (see figure 1), a as the side of one bond-fluctuation lattice cell, and $k_{\mathrm{B}}T$ as the unit of thermal energy, we define a dimensionless measure of the field strength $\varepsilon = (aqV)/(Lk_{\mathrm{B}}T)$. The speed $v(\varepsilon, N)$ of the molecules (where N stands for the molecular size) and their electrophoretic mobility

$$\mu(\varepsilon, N) = v(\varepsilon, N)/\varepsilon \tag{1}$$

then follow as the basic quantities we use to assess the separation capability of the device. We denote by μ_0 the mobility of the molecules in free solution (in a channel without constrictions), which is independent of field strength and molecular size.

A theoretical model has been proposed by Han et al. [1] for the motion of long polyelectrolytes driven by a dc electric field in their microchannel device. Taking $\overline{\tau}$ as the mean trapping time at the entrance of the narrow gap and t_{tr} as the time it takes to travel over one period L of the channel (in the absence of trapping), they write the intuitive relationship:

$$\frac{\mu(\varepsilon, N)}{\mu_0} \sim \frac{1}{1 + \overline{\tau}/t_{\mathrm{tr}}} \,. \tag{2}$$

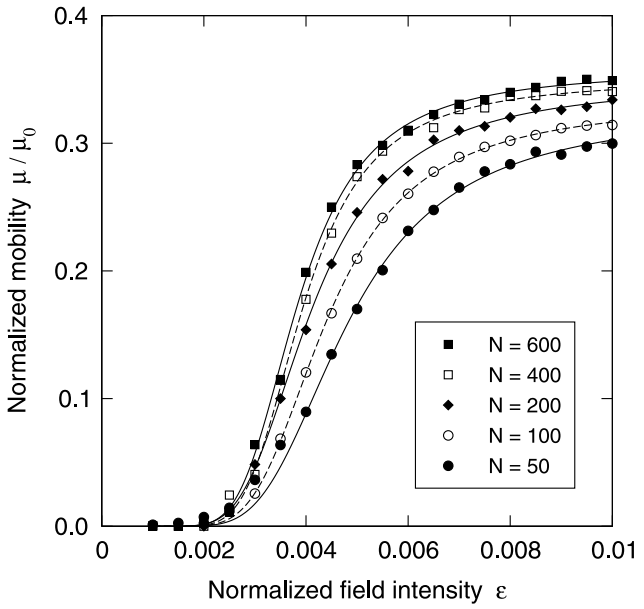

Figure 2: The normalized mobility as a function of the dc driving field strength. The curves are fits to the simulation data points using eq 4.

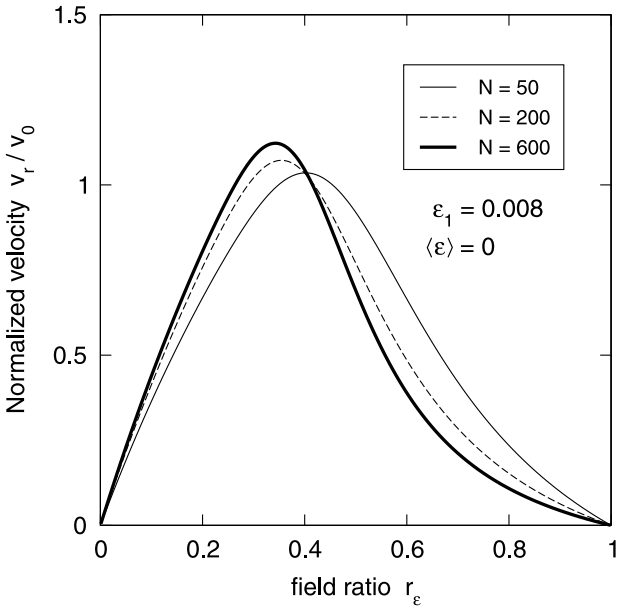

Figure 3: Velocity of macromolecules in a symmetric channel with a ZIFE driving field pulse (in the zero-frequency limit), as a function of the field ratio r_ε, for $\varepsilon_1 = 0.008$.

Obviously, $t_{\rm tr} \sim 1/\varepsilon$ for simple electrophoretic drift. Based on entropic trapping arguments, Han et al. also derive [1] the approximate relation

$$\overline{\tau}(\varepsilon, N) \approx \overline{\tau}_0(N)\, e^{-\kappa/\varepsilon} \; . \tag{3}$$

To our knowledge, no theory has been put forth to account for the migration behavior of the molecules when subjected to an ac driving field in this type of channel. In the next section, we build upon our dc results to calculate the velocity of the molecules in the ac case in the zero-frequency limit and we propose a phenomenological model to explain finite-frequency simulation results.

3 RESULTS AND DICUSSION

3.1 dc regime

Simulation results for the mobility of the polyelectrolytes in the microchannel are shown in Figure 2, as a function of the applied dc field strength. Each set of points corresponds to a different molecular size, and we see that longer molecules migrate faster than shorter ones, in agreement with experimental observation [1,2]. We can describe our simulation results quite well with a variant of eq 1 where we allow some additional dependence on the molecular size, namely:

$$\frac{\mu(\varepsilon, N)}{\mu_0} = \frac{\alpha(N)}{1 + \beta(N)\, \varepsilon\, e^{\,\kappa(N)/\varepsilon}} \; . \tag{4}$$

By fitting our data with such a function, we obtain an appropriate set of parameters (α, β, γ) for each molecular size. We forego discussing the meaning of the N dependence of these parameters, since our main goal here is to obtain an analytical representation of our data. In what follows we use these functions to compute velocities in the zero-frequency ac limit.

3.2 ratchet regime

The curves in Figure 2 show that the velocity of the molecules inside the channel does not increase linearly with field strength (in which case μ would be constant). This implies that we can operate the device in the ratchet mode, in which we can impart net motion to the molecules with a null time-averaged force. Consider a square pulse of the type used in zero-integrated-field electrophoresis (ZIFE) [5,6]: periodically, a field of strength $\varepsilon_1 > 0$ and duration t_1 is followed by a field of strength $\varepsilon_2 = -r_\varepsilon \varepsilon_1$ and duration $t_2 = t_1/r_\varepsilon$, where $0 < r_\varepsilon < 1$. We verify that the net applied field $\varepsilon_{\rm net} = (\varepsilon_1 t_1 + \varepsilon_2 t_2)/(t_1 + t_2)$ indeed vanishes.

In the limit of long t_1 and t_2, we can resort to our dc fits to calculate the velocity of the molecules under such conditions, since both sections of the square pulse correspond to a dc situation. Using indices 1 and 2 to refer to the first and second part of the pulse respectively, and realizing that $\mu(\varepsilon, N) = \mu(-\varepsilon, N)$ owing to the symmetry of the channel, we write the velocity of the molecules in the ratchet mode as:

$$\begin{aligned} v_{\rm r} &= \frac{\mu(\varepsilon_1, N)\varepsilon_1 t_1 + \mu(\varepsilon_2, N)\varepsilon_2 t_2}{t_1 + t_2} \\ &= \frac{\varepsilon_1}{1 + 1/r_\varepsilon} \left[\mu(\varepsilon_1, N) - \mu(\varepsilon_1 r_\varepsilon, N) \right] . \end{aligned} \tag{5}$$

In Figure 3 we plot $v_{\rm r}$ as a function of r_ε for $\varepsilon_1 = 0.008$ and three values of N. In our graphs we normalize veloci-

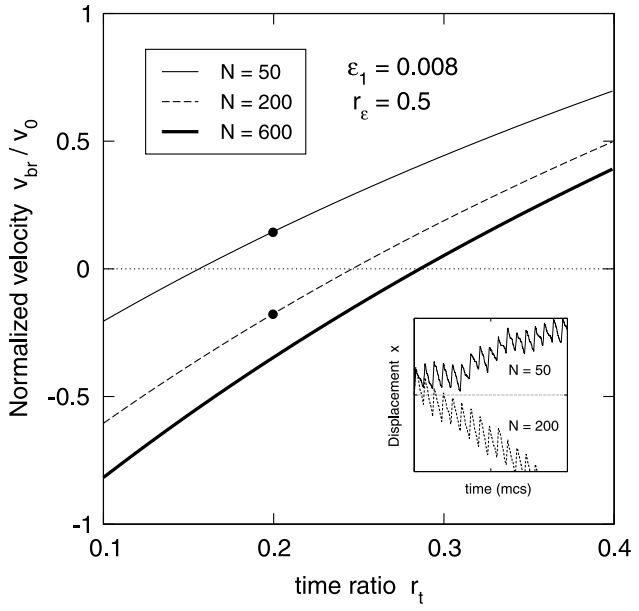

Figure 4: Normalized velocity of the macromolecules in a symmetric channel and a biased ratchet driving field, as a function of $r_{\rm t}$, for $\varepsilon_1 = 0.008$ and $r_\varepsilon = 0.5$. The inset, showing the actual displacement of molecules of sizes 50 and 200 as a function of time during an explicit low-frequency simulation with $r_t = 0.2$ (corresponding to the black dots in the main figure), confirms bidirectional transport.

ties with respect to $v_0 = 2\times10^{-5}\,\mathrm{a/mcs}$ (which is a typical velocity of the molecules in the best dc separation region around $\varepsilon = 0.004$). We first observe that the molecules indeed acquire a significant velocity under zero net force and that $v = 0$ when $r_\varepsilon = 1$, as required by symmetry. But the most striking feature of Figure 3 is that the elution order of the different molecular sizes, or bands, can be reversed compared to the dc case.

This inversion is most interesting, as we can exploit it in the following way. Suppose we bias the ZIFE pulse slightly in the negative direction (the direction of $\varepsilon_2 < 0$). This bias will reduce the net drift of the molecules, and we therefore expect the curves in Figure 3 to shift down vertically. Since the dc electrophoretic drift is more important for large molecules than for small ones, the curves will remain separated and will cross zero at different points. Hence *the net drift direction will depend on molecular size*. One way to impose such a bias is to modify the original ZIFE pulse to take longer strides in the direction of ε_2. Defining a new ratio $r_{\rm t} = t_1/t_2$ and following a similar derivation as in eq 5, we obtain an expression for the velocity of the molecules in the biased ratchet:

$$v_{\rm br} = \frac{\varepsilon_1 r_{\rm t}}{1+r_{\rm t}}\left[\mu(\varepsilon_1,N) - \frac{r_\varepsilon}{r_{\rm t}}\mu(r_\varepsilon\varepsilon_1,N)\right] \qquad (6)$$

In Figure 4 we plot $v_{\rm br}$ as a function of $r_{\rm t}$, for $\varepsilon_1 = 0.008$, $r_\varepsilon = 0.5$, and three values of the molecular size N. We find that for an appropriate choice of $r_{\rm t}$ the $N = 50$ and $N = 200$ molecules, for example, move in opposite directions (see figure inset). More significantly, it becomes possible to elute the different bands *one by one* by sweeping across a range of $r_{\rm t}$ values during a separation, a feature that may dramatically improve the separation capability of the device, especially if the latter is used for preparative electrophoresis.

3.3 finite frequency ac regime

In order to investigate the finite-frequency ac response of the system, we collect data from simulations in which the electric field explicitly follows a square pulse of period T that alternates between two positive field values (T is not to be confused with temperature, which in our context only appears in the factor definition of the dimensionless field intensity ε). We choose $\varepsilon_1 = 0.007$ and $\varepsilon_2 = 0.003$, for a net global field $\varepsilon_{\rm net} = (\varepsilon_1+\varepsilon_2)/2 = 0.005$. Out of the many time scales in the system, the one most likely to harbor a resonance in the drift velocity lies around $2\,\overline{\tau}(\varepsilon_1,N)$, i.e. twice the mean trapping time at $\varepsilon = \varepsilon_1$. Indeed, if $T/2 < \overline{\tau}$, then the probability that a molecule escapes during the most favorable ε_1 half of the pulse period is greatly reduced. However if $T/2 > \overline{\tau}$, then the pulse becomes unnecessarily long and the overall drift is reduced (unless of course the pulse is long enough for many barriers to be crossed in a single pulse cycle; since the standard deviation in trapping time $\sigma(\tau) \sim \overline{\tau}$, as derived below, these "harmonics" cannot be seen). Based on these observations, we can build a simple phenomenological equation for the dependence of the drift velocity on the pulse period:

$$v_{\rm ac}(T) \sim \mathrm{Prob}(\tau < T/2)\,\frac{L}{T}\,. \qquad (7)$$

The first factor in eq 7 is the probability that the trapping time in any given trap is less than half the period, which increases with T. The second factor is inversely proportional to T and embodies the waste of time due to unnecessarily long pulses. Here we assume that the molecule may only escape from the trap during the ε_1 part of the pulse and we disregard trapping times longer than T (associated, for example, with additional delays of T, $2T$, $3T$, etc. when the molecules fails to escape repeatedly). In that sense this is a first order model.

To find the position of the resonance peak from eq 7, i.e. the value T_0 for which the velocity is maximized, we must calculate $\mathrm{Prob}(\tau < T/2)$, hence we need to know the probability density function of the trapping time τ. From dc simulation data (not shown) we find that the distribution of trapping times is generally well approximated by the normalized distribution

$$\rho(\tau) = 2\,(\tau/\tau_{\rm c}^2)\,e^{-(\tau/\tau_{\rm c})^2}\,, \qquad (8)$$

where $\tau_{\rm c}^2 = 4\,\overline{\tau}^2/\pi$. From $\rho(\tau)$ we calculate $\mathrm{Prob}(\tau < T/2) = (1 - e^{-(T/2\tau_{\rm c})^2})$ and maximize $v_{\rm ac}(T)$ in eq 7 to

find the resonance condition $T_0^2 \approx 5\tau_c^2$, or

$$T_0 \approx \sqrt{\frac{20}{\pi}}\,\overline{\tau} \approx 2.5\,\overline{\tau}\,. \tag{9}$$

From the distribution in eq 8 we can also calculate $\sigma(\tau) = \sqrt{(4/\pi - 1)}\,\overline{\tau} \approx \overline{\tau}/2$; the distribution is thus quite broad. Consequently, we expect the resonance peak to be quite broad as well.

Finally, we can deduce the asymptotic behavior of the velocity far from the resonance region, for very long or very short periods T. When $T \gg \overline{\tau}$, we expect the velocity of the molecules to approach the mean of the velocities corresponding to each field intensity, hence we write:

$$\lim_{(T/\overline{\tau})\to\infty} \mu_{\rm ac} = \frac{\mu(\varepsilon_1, N)\,\varepsilon_1 + \mu(\varepsilon_2, N)\,\varepsilon_2}{2\varepsilon_{\rm net}}\,. \tag{10}$$

On the other hand, when $T \ll \overline{\tau}$, we expect to recover the mobility corresponding to the net global field $\varepsilon_{\rm net}$:

$$\lim_{(T/\overline{\tau})\to 0} \mu_{\rm ac} = \mu(\varepsilon_{\rm net}, N)\,. \tag{11}$$

Simulation results for the mobility of the molecules in the ac regime are presented in Figure 5 (the mobility is just proportional to the velocity here). Dashed lines indicate the long and short period limits calculated above, while for each molecular size an arrow points to the value of T_0 calculated from $\overline{\tau}$ (extracted from the dc data) according to eq 9. We see that the predictions for the asymptotic limits and for the position of the resonance peak are quite good. The separation is best for very short T, which corresponds to the dc case at a field $\varepsilon_{\rm net}$ which was chosen close to the optimum choice for dc separation. There is no inversion in the order of the bands, which makes sense since the driving field is always applied in the same direction. It is also clear from the graph that one cannot hope to single out a given molecular size by tuning into its resonant frequency, as the peaks for different molecular sizes are very broad.

The most interesting feature of the ac regime is that at the resonance the overall drift speed increases significantly (by as much as 30% for $N = 50$), while the separation of the different bands decreases only slightly. Hence it appears possible to increase the operating speed of this device while keeping the separation capability intact by means of an ac modulation of the dc driving field. We should note that we have studied only one amplitude of the ac modulation; the amplitude should also be examined as a variable to isolate the optimal separation scenario. It is quite possible that at optimal field intensity and ac amplitude one might actually obtain a performance exceeding that of the dc regime. This remains to be investigated further. Moreover, one might even add spatial asymmetry in the channel structure to further optimize the separation.

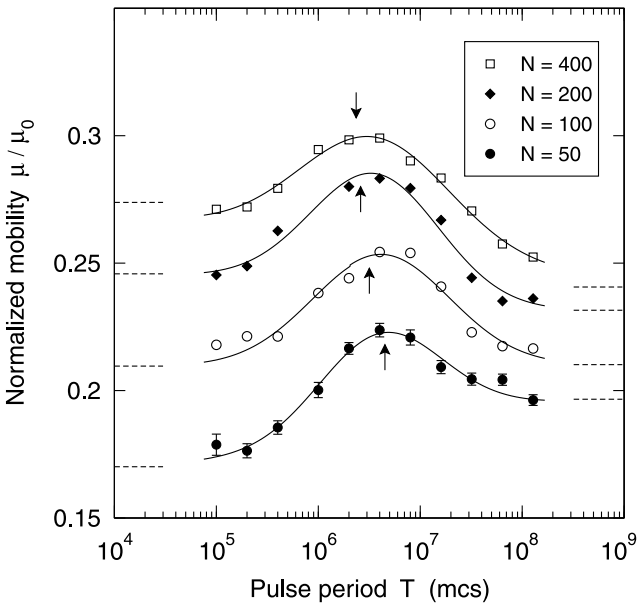

Figure 5: Mobility of macromolecules in a symmetric channel in the ac modulation regime, as a function of the driving field pulse period. The field oscillates between $\varepsilon_1 = 0.007$ and $\varepsilon_2 = 0.003$. The low and high-frequency limits, calculated from eq 10 and eq 11, are indicated by dashed lines on the right and on the left side of the graph respectively. The value of T_0 is indicated by an arrow for each molecular size. Solid lines are added to guide the eye.

REFERENCES

[1] J. Han, S. W. Turner, and H. G. Craighead, Phys. Rev. Lett. **83**, 1688 (1999).

[2] J. Han and H. G. Craighead, Science **288**, 1026 (2000).

[3] I. Carmesin and K. Kremer, Macromolecules **21**, 2819 (1988).

[4] H. P. Deutsch and K. Binder, J. Chem. Phys. **94**, 2294 (1991).

[5] G. W. Slater, H. L. Guo, and G. I. Nixon, Phys. Rev. Lett. **78**, 1170 (1997).

[6] G. A. Griess, E. Rogers, and P. Serwer, Electrophoresis **21**, 859 (2000).